Number	178
Publication Year	2022
Acceptance in OA@INAF	2022-08-19T07:53:27Z
Title	SRT performance measurements (2018-2021)
Authors	Egron, Elise; Vacca, V.; Carboni, G.; Pili, M.; Loru, S.; Castangia, P.; Pellizzoni, Alberto; SERRA, Giampaolo; IACOLINA, Maria Noemi; VALENTE, Giuseppe; ATTOLI, Alessandro; Buffa, F.; Mulas, S.; Perrodin, D.; Poppi, S.; Bachetti, M.; Burgay, M.; Caria, M. T.; Carretti, E.; Casu, S.; Concu, R.; Corongiu, A.; Deiana, G. L.; Fara, Antonietta; Gaudiomonte, F.; Ladu, A.; MARCHEGIANI, Paolo; MAXIA, PAOLO; Melis, A.; Milia, S.; Migoni, C.; Navarrini, A.; Orlati, A.; Ortu, P.; Palmas, S.; Pilia, M.; Pisanu, T.; SABA, Andrea; Schirru, L.; Soletta, P.; Surcis, G.; Tarchi, A.; URRU, Enrico; VARGIU, GIAN PAOLO
Affiliation of first author	O.A. Cagliari
Handle	http://hdl.handle.net/20.500.12386/32536; https://doi.org/10.20371/INAF/TechRep/178

SRT performance measurements (2018-2021)

E. Egron, V. Vacca, G. Carboni, M. Pili (1),
S. Loru (2), P. Castangia, A. Pellizzoni (1),
G. Serra, N. Iacolina, G. Valente, S. Mulas (3),
A. Attoli, F. Buffa, D. Perrodin, S. Poppi (1) et al. (#)

Abstract

Characterization tests are periodically performed at SRT in order to check the status of the antenna, ensure the correct functioning of the different components (e.g. active surface, receivers, backends, etc.), and improve the observing performances at the different frequencies. In particular, the tests include measurements of beam shape, pointing, gain curves and focus for the different receivers (L, C, X and K-bands).

We report the results of the main tests carried out after a long stop of the antenna due to the repair of the main servo motors chillers in 2020 and compare them with those carried out during the recommissioning in 2018 (after the change of the actuators of the active surface).

These results will be useful for comparing the new status of the antenna after the upgrade of the new receivers at higher frequencies (PON).

*****

(#) continued from cover page:

M. Bachetti, M. Burgay, M.T. Caria (1), E. Carretti (4), S. Casu, R. Concu, A. Corongiu, G.L. Deiana, A. Fara, F. Gaudiomonte, A. Ladu, P. Marchegiani, P. Marongiu, P. Maxia, A. Melis, S. Milia, C. Migoni, Navarrini (1), A. Orlati (4), P. Ortu, S. Palmas, M. Pilia, T. Pisanu (1), A. Saba (3), L. Schirru, P. Soletta, G. Surcis, A. Tarchi (1), E. Urru (3) and G.P. Vargiu (1).

(1) INAF - Osservatorio Astronomico di Cagliari
(2) INAF - Osservatorio Astrofisico di Catania
(3) Agenzia Spaziale Italiana (ASI)
(4) INAF - Istituto di RadioAstronomia di Bologna

Contents:

1) Introduction

Characterization tests (beam shape, pointing, focus and gain curves) are periodically performed for the different receivers at SRT in order to check the status of the antenna and improve the observing performances at the different frequencies. It is of utmost importance to carry out the tests after major antenna changes or repairs in order to ensure the correct functioning of the different components (e.g. active surface, receivers, backends, etc).

Observations at SRT were suspended for several months from February to September 2017 in order to change all of the actuators of the main reflector (M1)'s active surface. A period of recommissioning from September 2017 to May 2019 allowed us to check that the M1 active surface look-up table[1] (M1-LUT) was still working properly and to perform the characterization tests of the antenna performance.

Several holographic measurements were carried out before and after the active surface refurbishment. The resulting holographic maps of the M1 surface deformations are shown in Figure 1. Except for some actuators stuck in an unknown position (see blue large dots on the left panel), the two maps turned out to be very similar, showing a M1 surface alignment within 280 ± 20 μm rms.

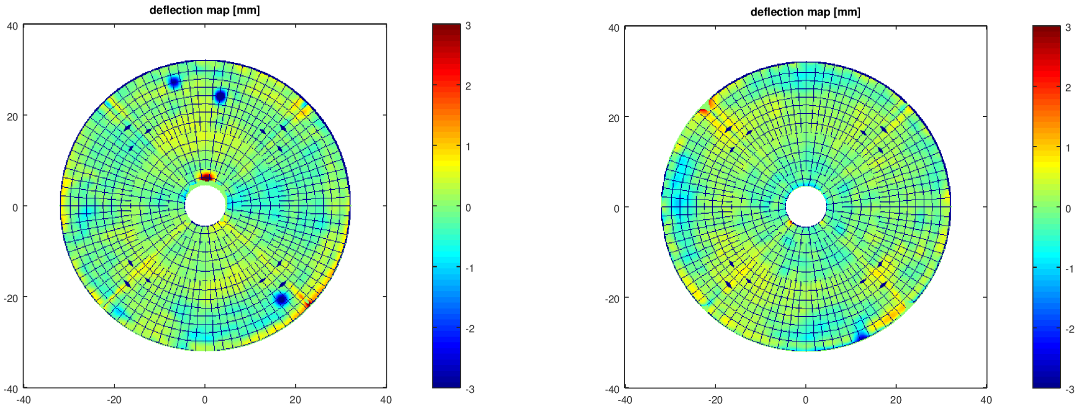

Figure 1: Holographic maps (in mm) of the M1 surface deformations pre-refurbishment (left) post-refurbishment (right).

This result confirmed that the M1-LUT, derived by the photogrammetry measurements (Süss et al. 2012 - MTM-SIGMA3D), is still accurate (within the holography measurement uncertainty) and ensures a very good antenna performance in terms of surface efficiency, at least up to 40 GHz.

We performed characterization tests from September 2020 to February 2021 in order to check the correct functioning of the antenna in parallel with the proper observations after the stop of SRT in April 2020 (due to some problems regarding the main servo motors chillers).

During these tests, the antenna setup was changed to allow the use of a new M1-LUT derived by more recent Out-Of-Focus (OOF) holography measurements performed at different elevations (Buffa et al. 2020). No changes were applied at the M2-LUT derived by laser scanner measurements (Süss et al. 2012 - MTM-SIGMA3D). The current M2-LUT still allows significant improvements in the M1-M2 axes alignment, except for a residual misalignment at lower elevations producing large scale deformations we are still investigating.

---

[1] The LUT is a table of numbers allowing for the real-time correction of the antenna structure deformations or misalignments. SRT uses two LUTS, one, a.k.a. M1-LUT, dedicated to the correction of the M1 gravitational surface deformations w.r.t. to the ideal shaped profile; the other one, a.k.a. M2-LUT, to correct for M1-M2 axis misalignment (M2-LUT) w.r.t. the antenna axis, both varying with the elevation.

Hereafter, we refer to a "new M1-LUT" as the LUT resulting from the M1-LUT derived by the photogrammetry measurements (Süss et al. 2012 - MTM-SIGMA3D) combined with the OOF holography results performed in 2020. The “new M1-LUT” was produced in order to correct for the large scale residual optical aberrations on the antenna aperture field resulting in the OOF maps, likely due to the M1 and M2 axes misalignments (not corrected by the M2-LUT). Since SRT is not yet provided with instrumentation able to implement a fine calibration of the M2-LUT, what we describe here is an attempt to compensate for such aberrations (corresponding to surface deformations on the aperture field of a few mm), with the M1 active surface whose actuators have a stroke equal to +/- 15 mm. We are not sure if this experiment will succeed, but it requires more attempts to figure it out.
In any way, a dedicated instrumentation to implement a fine calibration of the M2-LUT and support the current metrological system will be available after the SRT metrological system upgrade foreseen by one of the PON objectives (https://sites.google.com/a/inaf.it/pon-srt/).

The “New M1-LUT” are very preliminary and could need further observations to characterize them well. However, among the several purposes of the tests presented in this report, we also need to check if, at this early stage, there are some improvements in terms of beam shaping given by the introduction of the “new M1-LUT”. **Note that the scientific observations performed at SRT until July 2021 did not use the "new M1-LUT”.**

Observations at SRT were stopped in July 2021 in order to proceed with a major upgrade of the new receivers at higher frequencies (PON; Govoni et al. 2021). The results of our tests will be useful as a confrontation when we start with the new tests in 2022/2023.

The deep space SRT asset, a.k.a. Sardinia Deep Space Antenna, is managed by ASI and provides an X-band capability for the spacecraft signal downlink (Valente et al. 2022). Since 2017, SDSA has been operating in the frequency range 8.4-8.5 GHz thanks to a cryogenic receiver borrowed from NASA-JPL. Hosted on one of the SRT beam wave guide foci, this device can receive both circular polarizations, but only one at a time can be selected (RHCP or LHCP). **Although this asset is not available for the INAF "call for proposal"**, the tests aimed at the characterization of the antenna performances (beam shape, pointing accuracy and gain curve) at X-band are described here.

In the following sections, we present the characterization tests performed for the L, C, X and K band receivers (Valente et al. 2010; Orfei et al. 2011; Orfei et al. 2010). We compare the results of the tests carried out after September 2020 with the main results from the recommissioning (see Recommissioning report 2019).

2) Beam shape

The characterization of the beam shape in total intensity is an important tool for evaluating the possible variations/aberrations as a function of the elevation and for checking the pointing models for the different receivers.
The beam shape characterization was performed in C-band and K-band during the commissioning (Bolli et al. 2015; Murgia et al. 2016) and during the Astronomical Validation (AV; Prandoni et al. 2017). Below we compare these results with those obtained more recently during the recommissioning using the new pointing model (after the active surface actuators were replaced) in June 2018, and after the second stop of the antenna, in September 2020. We also present the beam shape in L-band, which is useful for the VLBI. Data reduction was performed using the Single Dish Imager software (SDI; PI Pellizzoni; Egron et al. 2017; Loru et al. 2019). A summary of the observations and schedule parameters is presented in Appendix A.

- **L-band**

We performed On-The-Fly (OTF) maps of Cygnus A in L-band with SARDARA (Melis et al. 2018) in horizontal coordinates from 23° to 35° el on 15/09/2020 and from 54° to 73° el on 03/11/2020. We increased the number of passages per beam from FWHM / 4 = 3.6' to FWHM / 8 = 1.8' for the second session so that more of the inner part of the beam is sampled, as required from the Joint Institute for VLBI ERIC (JIVE). The maps are presented in Fig.2 and parameters of the schedule are reported in Appendix A, in Table A.2. These maps are useful to check the consistency of the beam shape for the VLBI.
Note that due to the numerous RFI in L-band, we severely cleaned the SARDARA data. The central frequency results to be 1.4 GHz and the associated beam size is 14.2' (measured from the Gaussfit function on the final maps).

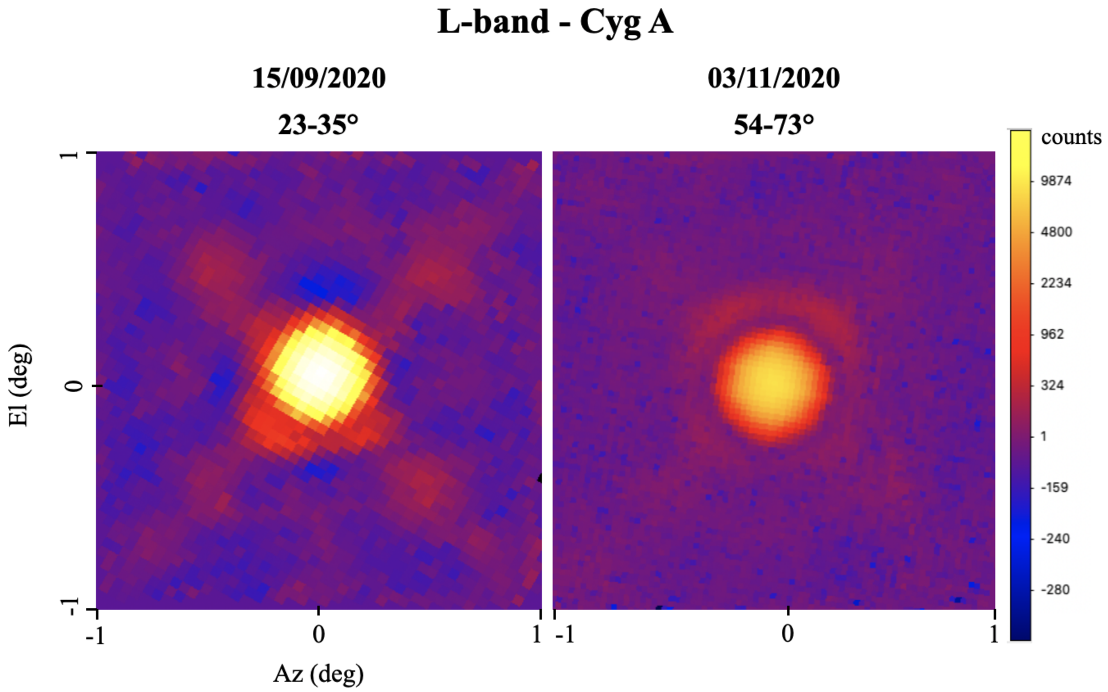

Figure 2: *Az/El maps of Cyg A obtained at 1.5 GHz with SARDARA on 15 September and 3 November 2020. The difference in the pixel resolution is due to the difference in the parameters of the schedule: 4 passages/beam (left) and 8 passages/beam (right). The beam size is 0.24°.*

- **C-band**

We performed OTF maps of the point-like sources 3C454.3, 3C345 and 3C84 in horizontal coordinates in order to estimate the beam size, beam deformations and relative counts in the secondary lobes w.r.t. the primary lobe. Note that 3C84 is one of the brightest but variable calibrators in C-band (about 30 Jy at 7 GHz), and it represents the most suitable target to perform the test in order to achieve our goals. Observations were carried out during the recommissioning at 7.2 GHz with the Total Power on 21/12/2017, 08/01/2018, 30/01/2018 and 04/04/2018. The beam shape test was then repeated at 7.0 GHz with SARDARA on 29/09/2020 and 07/11/2020 using the "*new M1- LUT*".

The maps of 3C84 obtained in 2018 and 2020 at the different elevation ranges are presented in Fig. 3 and 4, respectively. The second lobes and the quadripode are clearly detected on the maps. The second lobe is asymmetric at low and high elevations, as already noticed during the Astronomical Validation (Prandoni et al. 2017). Instead, it appears symmetric at 50-65° of elevation.

The counts or flux per beam associated with the central beam and the secondary lobes (maximum counts/flux in the second and third lobes) are reported in Tables 1 and 2 for the different elevation ranges of 3C84. The counts or flux density in the second lobes represent at maximum about 2.1% (second lobe) and 0.65% (third lobe) of the central beam.

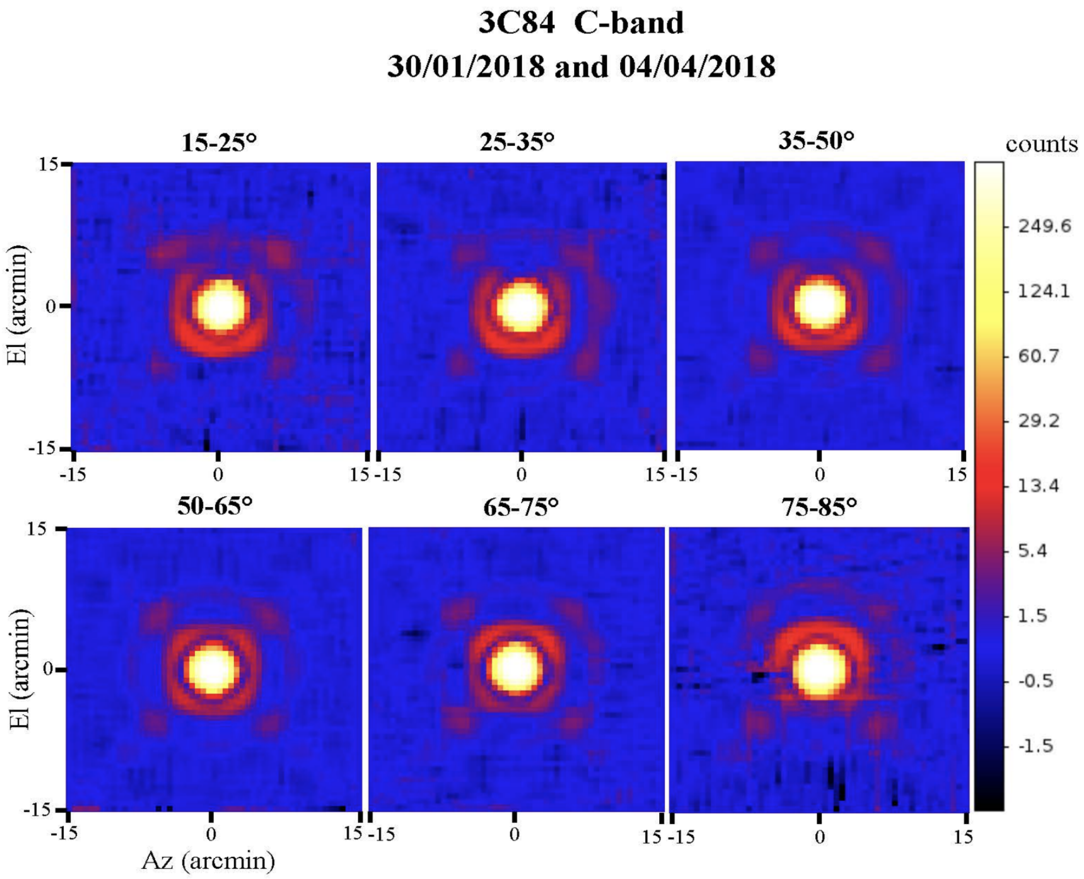

Figure 3: *Az/El maps of 3C84 obtained at 7.2 GHz with the TP during the recommissioning (2018).*

3C84 **7.2 GHz**	**Central beam** (max counts)	**Second lobe** (max counts) **(% cts w.r.t. central beam)** **(in dB)**	**Third lobe** (max counts) **((% cts w.r.t. central beam)** **(in dB)**
15-25°	460	8 **1.7%** **-17.6 dB**	3 **0.65%** **-21.9 dB**
25-35°	476	8 **1.7%** **-17.7 dB**	2 **0.42%** **-23.8 dB**
35-50°	486	7 **1.4%** **-18.4 dB**	2 **0.41%** **-23.9 dB**
50-65°	484	5 **1.0%** **-19.9 dB**	2 **0.41%** **-23.8 dB**
65-75°	465	7 **1.5%** **-18.2 dB**	2 **0.43%** **-23.7 dB**
75-85°	504	10 **2.0%** **-17.0 dB**	2 **0.40%** **-24.0 dB**

Table 1 : *Counts per beam associated with the central beam and the secondary lobes (maximum counts in the second and third lobes) for the different elevation ranges of 3C84 during the recommissioning (2018).*

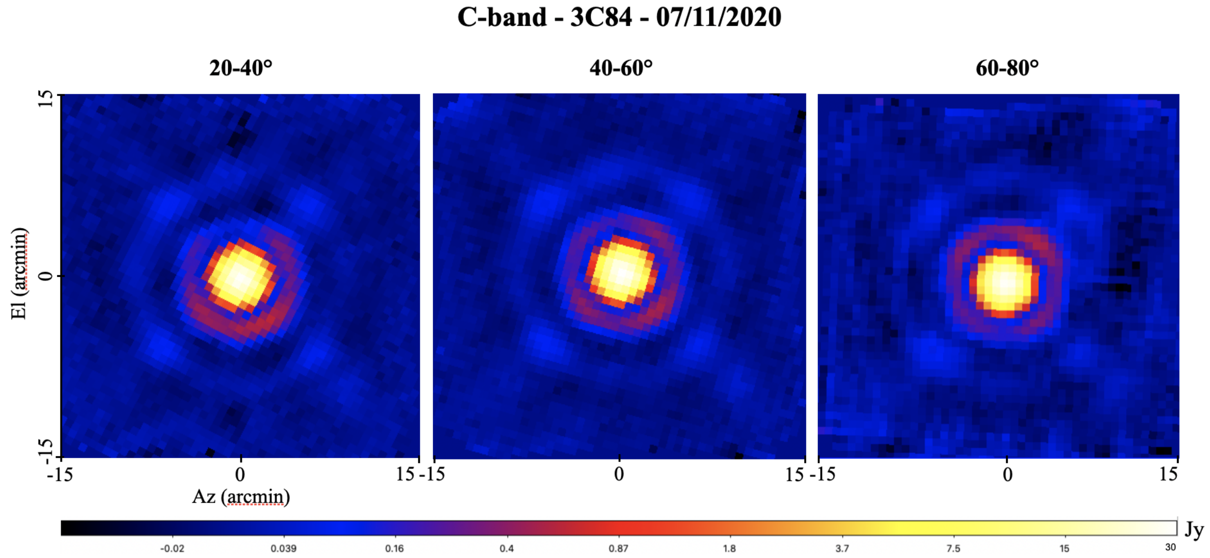

Figure 4: *Az/El maps of 3C84 obtained at 7.0 GHz with SARDARA on 7 November 2020.*

3C84 **7.0 GHz**	**Central beam** (Jy)	**Second lobe** (brightest pixel in Jy) **(% flux central beam)** **(in dB)**	**Third lobe** (brightest pixel in Jy) **(% flux central beam)** **(in dB)**
20-40°	28.9	0.60 **2.1%** **-16.8 dB**	0.097 **0.36%** **-24.7 dB**
40-60°	29.9	0.49 **1.6%** **-17.9 dB**	0.10 **0.33%** **-24.9 dB**
60-80°	28.5	0.50 **1.8%** **-17.6 dB**	0.12 **0.42%** **-23.8 dB**

Table 2 : *Flux density of 3C84 associated with the central beam and the secondary lobes (brightest pixel in the second and third lobes) for the different elevation ranges obtained at 7.0 GHz in 2020 (see Figure 3).*

The beam size gives reliable information on the optics of the telescope and on the good functioning of the active surface and tracking subreflector. The beam deformation (ε) with respect to the estimated HPBW (beam size, θe) is calculated as follow:

$$\varepsilon = \sqrt{(\theta_{\rm az} - \theta_e)^2 + (\theta_{\rm el} - \theta_e)^2}.$$

where θaz and θel are the beam sizes measured along the azimuth and elevation axis, respectively (Bolli et al. 2015).

We measured the beam size for the different sessions (2018 and 2020) by fitting each single map of the calibrators in azimuth and elevation with a 2D Gaussian function. The beam size and beam deformations in C-band are shown in Fig. 5 and 6 and appear consistent with the measurements reported during the AV and the technical commissioning.
In 2018, the mean value of the beam size was 2.64’ at 7.24 GHz, with a slight increase at low elevation (< 20°), as shown in Fig. 5. For a comparison, the theoretical beam size at such frequency is 2.62’. In 2020, we obtained a mean beam size of 2.77 +/- 0.02 arcmin at 7.0 GHz. We observed a slight deviation from this trend at low (< 20°) and high (>70°) elevations. Our measurements are within the 10% deviation from the theoretical value (2.71’ at 7.0 GHz), even if they are slightly above this

value. The beam shape is instead mostly consistent with the theoretical value around 65° of elevation, as expected from the SRT optimized performances at these elevations.

We also measured the beam deformation in azimuth and elevation at the various elevations (Fig. 6). In 2018, a deformation of 0.084' +/- 0.054' is found at all the elevations, which corresponds to 3% of the beam. In 2020, we measured a mean beam deformation of 0.127’ +/- 0.048’ (5% of the beam). The beam shape as a function of the elevation indicates an increased spread above ~60°. For a comparison, the deformation was about 0.18' at 7.35 GHz before the change of the actuators (Bolli et al. 2015), as illustrated in Fig. 7.

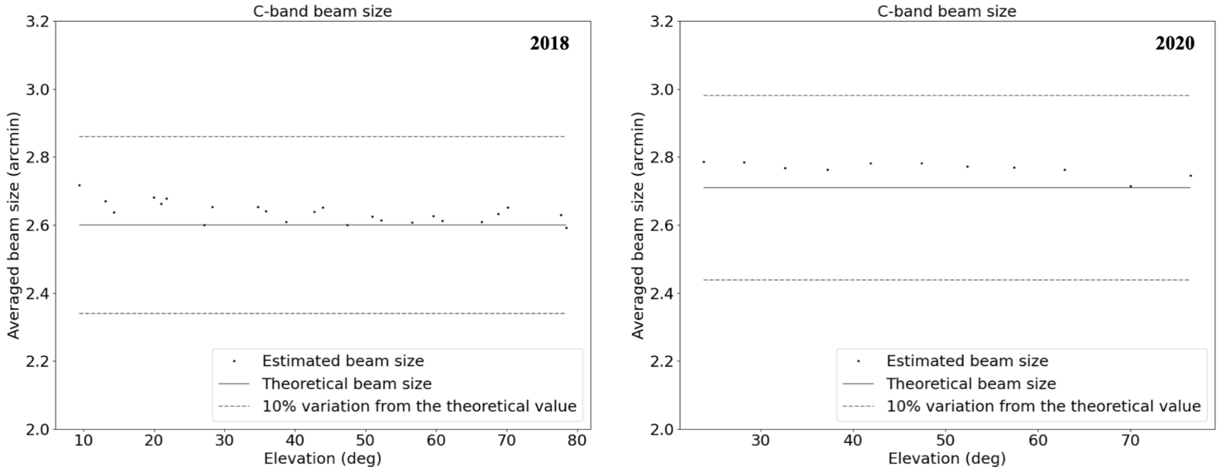

***Figure 5:** C-band beam size as a function of the elevation corresponding to 3C454.3, 3C345 and 3C84 in 2018 (left) and 3C84 in 2020 (right). The solid line indicates the theoretical beam size value rescaled from Bolli et al. (2015) at the central frequency 7.24 GHz (left) and 7.0 GHz (right), while the dashed line indicates the 10% deviation from the theoretical value.*

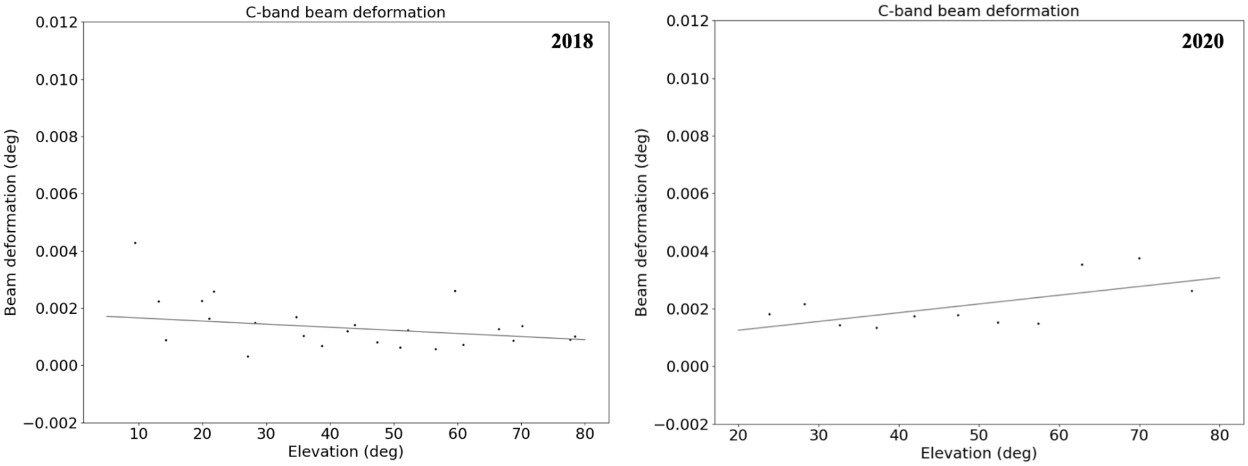

***Figure 6:** C-band beam deformation for the different elevation ranges measured at 7.24 GHz during the recommissioning in 2018 (left) and at 7.0 GHz in 2020 (right).*

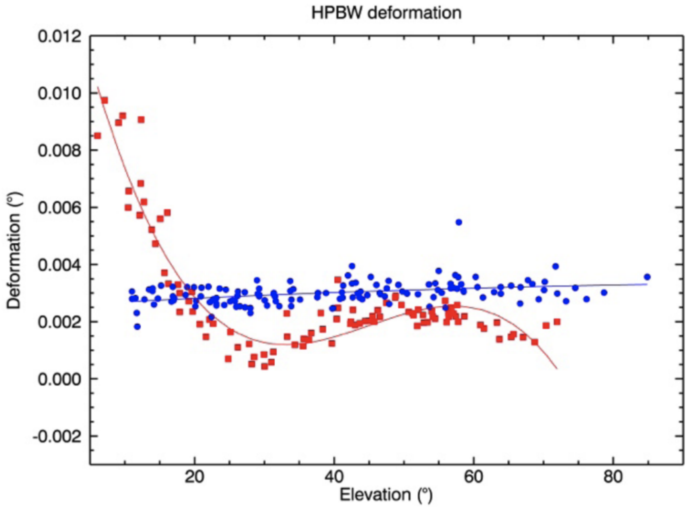

Figure 7: *C-band beam deformation obtained by Bolli et al. (2015) at a central frequency of 7.35 GHz and a related beam size of 2.58'. Red squares and blue circles indicate data obtained with (i) a fixed optics and (ii) with the active surface plus tracking subreflector, respectively.*

- **X-band**

We carried out observations for the beam shape analysis of the X-band receiver on 23 March 2021. The right polarization was selected for the observations described in the following.
We observed the pointing calibrator source 3C84 during the 15:30 – 22:45 UTC time range from 7° to 77° of elevation. The observing strategy included the following procedure: a) Cross-scans on various pointing and flux calibrator (at the beginning and at the end of the session); b) Pointing procedure on 3C84 for pointing correction; c) Focus procedure on 3C84 for focus correction; d) Az-El maps on 3C84. Points b), c) and d) were repeated during all the observing time range. Details of the observation are listed in Table 3.

Obs Parameters	Value	Obs Parameters	Value
Obs Date	23/03/2021	Weather Condition	Cloudy – Variable
Obs time range	15:30-22:45 UTC	wx	10.4, 52.6, 949.4, 13.7
Obs Frequency	8.45 GHz	**Map Parameters**	**Value**
Polarization	Right	Radio source	3C84
Bandwidth	28 MHz	Map size	0.5d x 0.5d
Backend	TP	Scan Interleave	0.001d
Schedule Frame	Horizontal	Antenna velocity	4 deg/min
HPBW X-band	0.0381° – 2.2869'	Map Color Scale	Log

Table 3 : *Observing and map parameters for the 23/03/2021 session for beam shape analysis at X- band.*

We obtained 11 3C84 Az-El maps (0.5d x 0.5d size). Each map covered an elevation range of about 5°. For each map we performed a 2d Gaussian fit obtaining the peak and the HPBW, and we measured the background counts rms. Moreover, as the maps were very clean and with high exposition (antenna velocity of 4 deg/min), the side lobes were very clear and we measured count peaks of the second, the third and the fourth lobe (even if the last one was often represented by only few brighter pixels in the background). Results of the analysis are reported in Table 4.

3C84						
Elevation range (°)	**Ref El (°)**	**1st Lobe S/N[a] (dB)**	**2nd Lobe[b] (dB)**	**3rd Lobe[c] (dB)**	**4th Lobe[d] (dB)**	**Deformation[e] (°)**
07 – 11	9	27.1	-16.4	-21.3	-20.5	0.0134
11 – 16	14	28.3	-16.7	-21.7	-23.7	0.0030
17 – 22	20	28.6	-15.3	-21.1	-24.8	0.0026
22 – 28	25	29.1	-14.9	-21.5	-24.9	0.0020
28 – 34	30	29.5	-14.8	-22.0	-24.8	0.0023
34 – 40	35	29.4	-15.6	-21.6	-24.4	0.0023
41 – 47	45	29.6	-16.8	-21.5	-24.8	0.0027
47 – 54	50	30.0	-17.7	-21.7	-25.3	0.0033
54 – 61	58	30.3	-17.8	-22.4	-24.1	0.0032
62 – 69	66	30.2	-18.1	-21.4	-24.4	0.0034
70 – 77	74	29.9	-17.1	-20.7	-24.0	0.0034

Table 4 : *Results of the data analysis, see the text for the description of the various columns.*

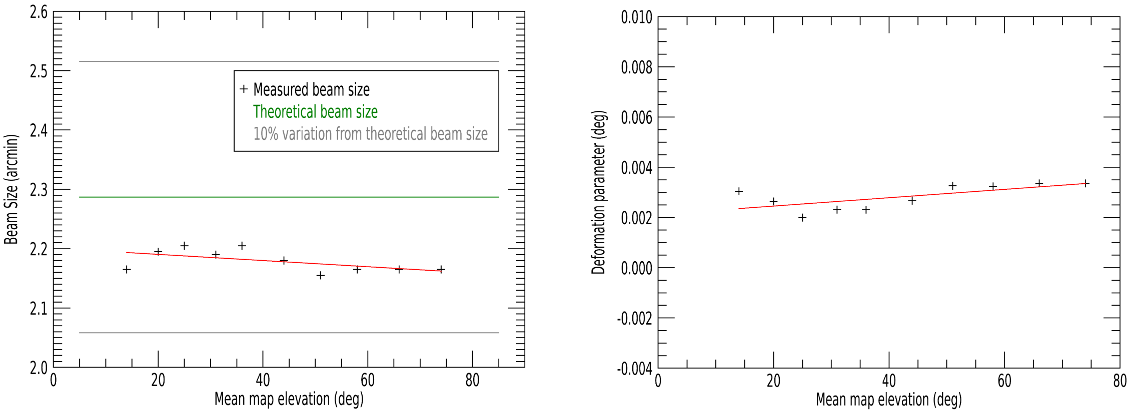

Figure 8: *Left: beam size in arcmin versus elevation (degrees). The red line represents the linear fit, green line represents the theoretical value (2.2869'), grey lines indicate the 10% variation from the theoretical value. Right: HPBW deformation parameter versus elevation angle (both in degrees). The red line represents the linear fit. Values and behavior with respect to the elevation are compatible with values and behavior at C-band reported in Bolli et al. (2015).*

The resulting beam size is shown in the left panel of Fig. 8. The green line in the plot represents the theoretical value, while the gray lines indicate the zone inside the 10% of the theoretical beam size. The mean beam size resulted in 2.18±0.03 arcmin.

The deformation parameter was calculated through the 2D gaussian fit parameters, using the formula:

$$\varepsilon = \sqrt{(\theta_{\mathrm{az}} - \theta_e)^2 + (\theta_{\mathrm{el}} - \theta_e)^2}.$$

where θ_az and θ_el are the HPBWs of the 2d gaussian fit and θ_e is the theoretical HPBW (1.22 λ/D=0.0381°). The mean beam deformation is 0.17±0.04 arcmin, which corresponds to about 7.5% of the beam size.

The result is shown in the right panel of Fig. 8 and is comparable with that shown in Bolli et al. (2015) for the C-band. SNR calculated for each map is represented by the ratio between the peak of the gaussian fit and the rms of the measurement background noise. That is shown in the left panel of Fig. 9, where the red line indicates the 2nd order fit. Note that the values are indicated in dB. The right panel of Fig. 9 shows the behavior of the sidelobes' peak value with respect to the elevation. Colored solid curves indicate the 2nd order fit. Values related to the secondary lobe seem not to meet the SRT specification requirement, as they should not be higher than -20 dB at all elevations**.**

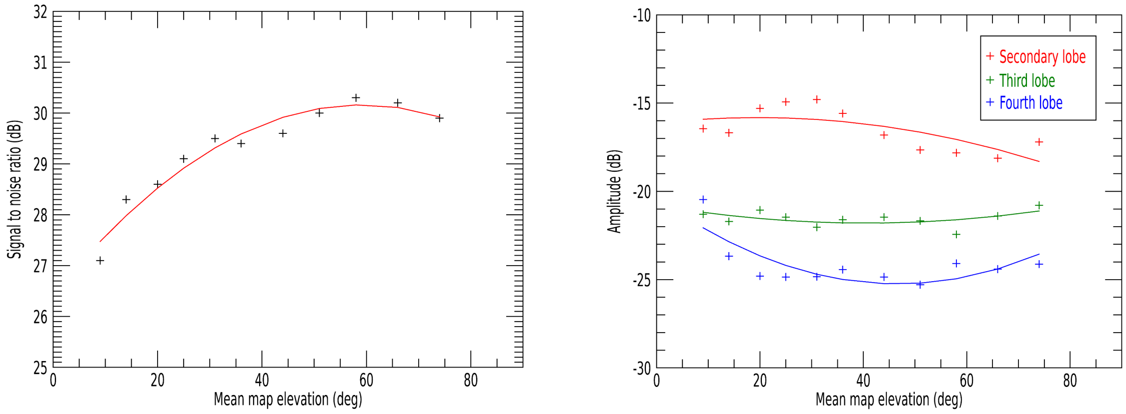

Figure 9: Left: *Signal to noise ratio of the main peak (dB) versus elevation angle (degree)*. Right: *2^{nd}, 3^{rd} and 4^{th} lobe* w.r.t. 1^{st} lobe peak *(dB) versus elevation angle (degrees). Colored lines represent 2^{nd} order fits. Values of the 4^{th} lobe curve (the blue one) were represented by only a few brighter pixels in the map background.*

We present the flux density of the source 3C84 versus the elevation in the left panel of Fig. 10, considering a value of 4.68±0.05 Jy for the 3C147 calibrator at 8450 MHz (Perley and Butler 2017). The blue dots in the plot represent values corrected for the gain curve, while gray dots indicate raw values. The blue and gray solid lines indicate the 2nd order fit, but what appears to be a parabolic trend is only due to measure dispersion and is not correlated to the elevation. Measured values do not represent a reference for the flux density of the source as it is a strongly variable radio source (Britzen et al. 2019). Calibrated map rms (in Jy) is shown in the right panel of Fig. 10. As expected, values are higher at lower elevation. The maps are shown at the various elevations in Fig. 11.

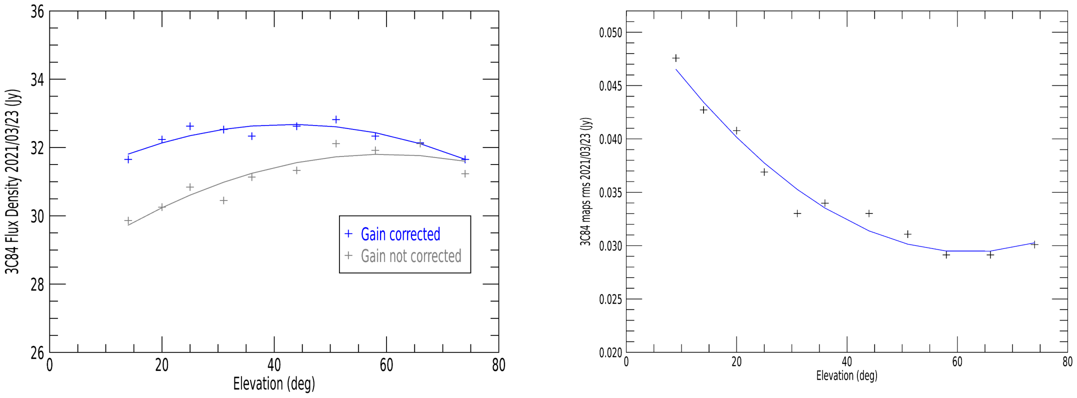

Figure 10: *Left: Flux density (Jy) for 3C84 related to the elevation values spanned during observations. The blue curve indicates values corrected for gain curve, while the gray curve refers to values not corrected for the gain curve (flux density values are not valid as a reference for flux calibration). The blue and gray solid lines represent the 2^{nd} order fit. Right: rms value (Jy) of the 3C84 maps taken at the various elevation. The blue line represents the 2^{nd} order fit.*

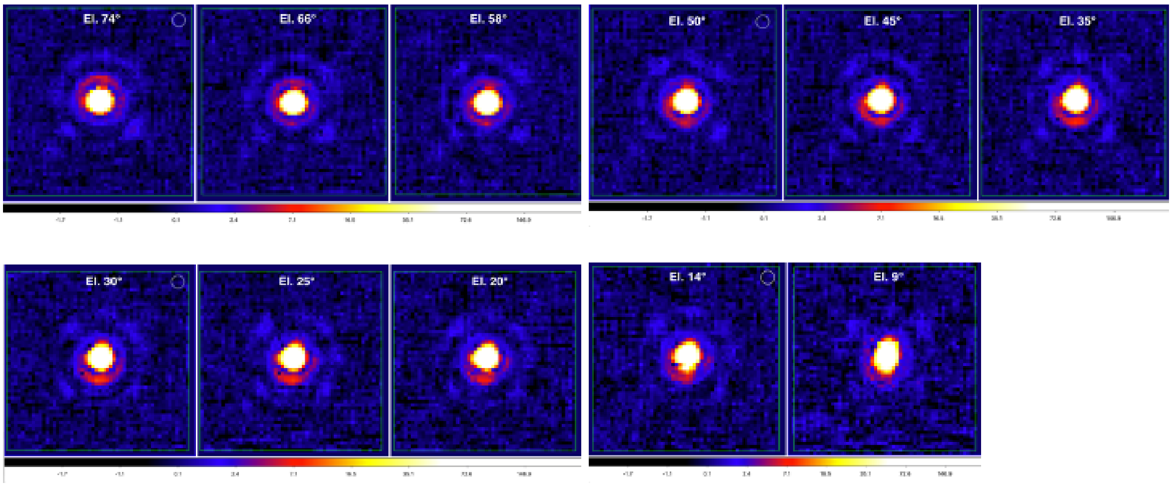

Figure 11: *Maps of 3C84 at high, mean, low and very low elevations, taken on 23/03/2021 at 8.45 GHz.*

- Cross scan pointing Offsets

Fig. 12 shows the Az-El offset behavior related to the cross-scans performed before each map during all the session. The offset values stay almost always within a tenth of the HPBW, in agreement with the pointing error requirement, thus validating the current pointing model.

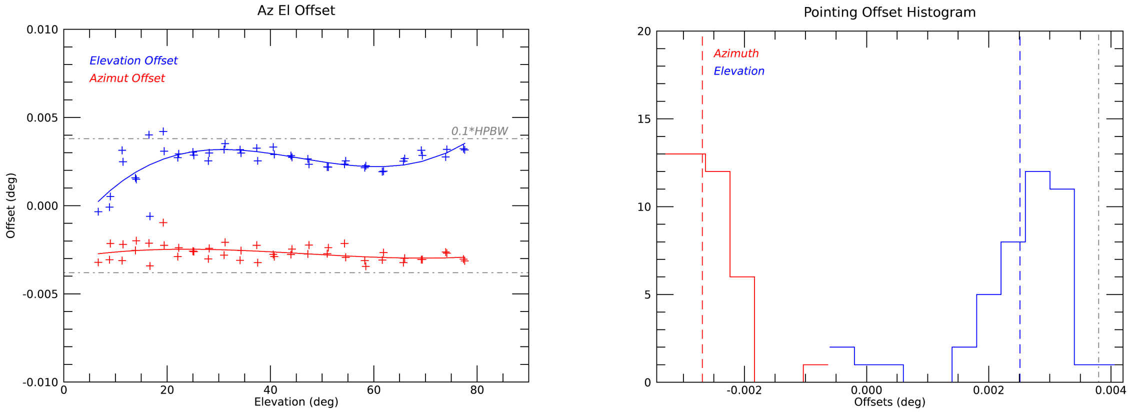

Figure 12: *Left: cross scan offsets taken during all the beam shape sessions versus elevation. Coloured solid lines represent the fit curve (3rd order). Right: histogram of the cross-scan offsets. Vertical coloured lines represent the mean values. Dash-dotted grey lines indicate the value of a tenth of the HPBW (the standard reference value for the pointing error).*

- **K-band**

We performed OTF maps of the point-like source 3C84 in Az/El in order to estimate the beam size, beam deformations and relative counts in the secondary lobes w.r.t. the primary lobe. Note that the radio galaxy 3C84 (NGC1275) is not a flux calibrator since it shows flux variations on the scale of the month (Britzen et al. 2019). However, it is one of the brightest point-like sources in K-band, which allows us to clearly see the secondary lobes during a single session. The observations were carried out during the recommissioning on 03/09/2018 at 22 GHz (central frequency) with the Total Power. The weather was clear during the observations. We produced pairs of Az/El maps of 3C84 at different elevation ranges from 9 to 82°.

As expected, maps obtained at 9-12°, 12-15° and 16-19° of elevation present a strong asymmetry, in particular the map at 9-12°, as shown in Fig. 13. Indeed, the LUT of M1 and M2 were created from photogrammetric measurements carried out in the 15-80° elevation range. The correction values of M1 and M2-LUTs at lower elevation are extrapolated and imprecise values. This explains the significant beam asymmetries at elevations below 15°. For higher elevations, we begin to see the corrective effect of the LUTs on the beam.

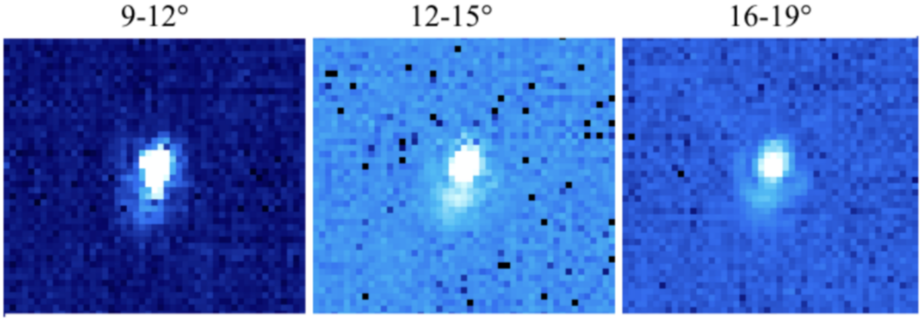

Figure 13: *Maps of 3C84 (0.2°x0.2°) obtained at 22.0 GHz on 03/09/2018 at 9-12°, 12-15° and 16-19° of elevation, respectively.*

We then summed the maps corresponding to 20-40°, 40-60° and 60-80° of elevation in order to increase the S/N and detect the secondary lobes. The resulting maps are presented in Fig. 14. The second lobe is asymmetric, in particular at low and high elevations, as already noticed during the AV (Prandoni et al. 2017). This is due to the misalignment of the M2 axis w.r.t. the M1 one, which produces optical aberrations. The counts in the secondary lobes represent at maximum 11% of the central beam, between 20° and 40° of elevation, and less than 5% above 40°. The third lobe, instead, is always less than or equal 0.6% of the central beam. The details of the counts in the central and secondary lobes at the different elevations are reported in Table 5.

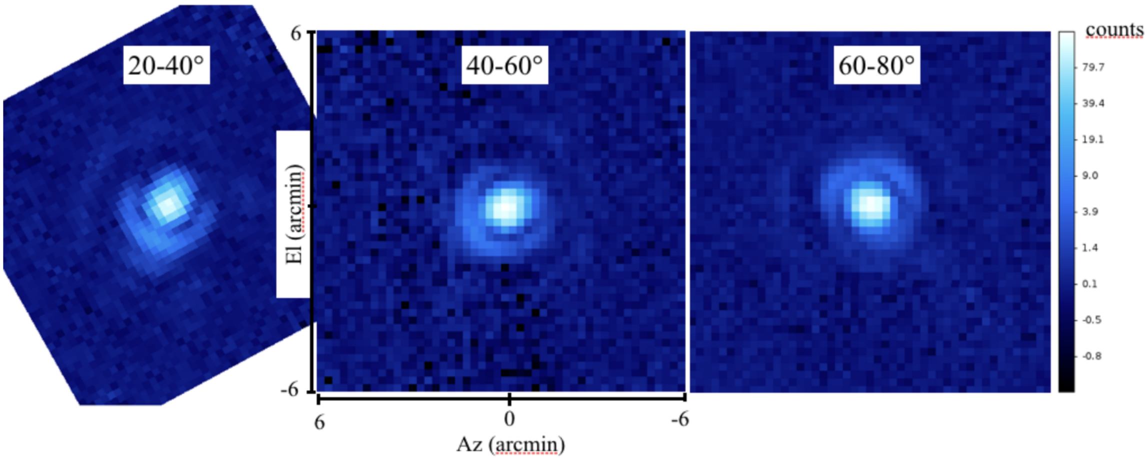

Figure 14: *Az/El maps of 3C84 at 22.0 GHz in counts/beam at 20-40°, 40-60° and 60-80° of elevation (see Table 5) obtained in 2018 during the recommissioning, with a pixel resolution of 0.25'.*

3C84 **22.0 GHz**	**Central beam** (max counts)	**Second lobe** (max counts) **(%cts w.r.t. central beam and in dB)**	**Third lobe** (max counts) **(%cts w.r.t. central beam and in dB)**
20 – 40°	127	14 **11%** **-9.6 dB**	0.7 **0.6%** **-22.6 dB**
40 – 60°	163	8 **4.9%** **-13.1 dB**	0.8 **0.5%** **-23.1 dB**
60 – 80°	147	5 **3.4%** **-14.7 dB**	0.7 **0.5%** **-23.2 dB**

Table 5 : *Counts per beam of 3C84 associated with the central beam and the secondary lobes (maximum counts in the second and third lobes) for the different elevation ranges (see Figure 14).*

Beam shape sessions on 3C84 were repeated in September 2020 (20-40°el) and in December 2020 (20-80°el) at 18.7 GHz (central frequency). The data obtained in December 2020 were also used to test the sensitivity of the channels for the 7 feeds of the receiver. We used the Total Power (TP) for the pointing, focus and skydip, and SARDARA to perform the maps on the target. The derotator was set in the fixed configuration with an angle of 0°. The parameters of the schedules are reported in Appendix A.

We present in Fig. 15 the maps of 3C84 obtained on 14 September 2020 at 20-30° and 30-40°el, calibrated by performing cross-scans on 3C286 at 46° and 53°el (2.9 Jy at 18.7 GHz). In Fig. 16, we show the maps produced on 17-18 December 2020 using the *“new M1 LUT”* (Buffa et al. 2020) at 20-40°, 40-60° and 60-80° of elevation, calibrated with cross-scans on 3C147 at 57°, 61° and 66°el (2.1 Jy at 18.7 GHz). Asymmetries of the second lobe are observed at low and high elevations. In Fig. 17 we show the profile of the central scans of the maps in azimuth *(top)* and elevation *(bottom)* at 20°, 40°, 60° and 80°elevation. The second lobe is clearly evident at 20°, 40° and 80° elevation during the scans in elevation, while the profile of the scan is symmetrical at 60°elevation.

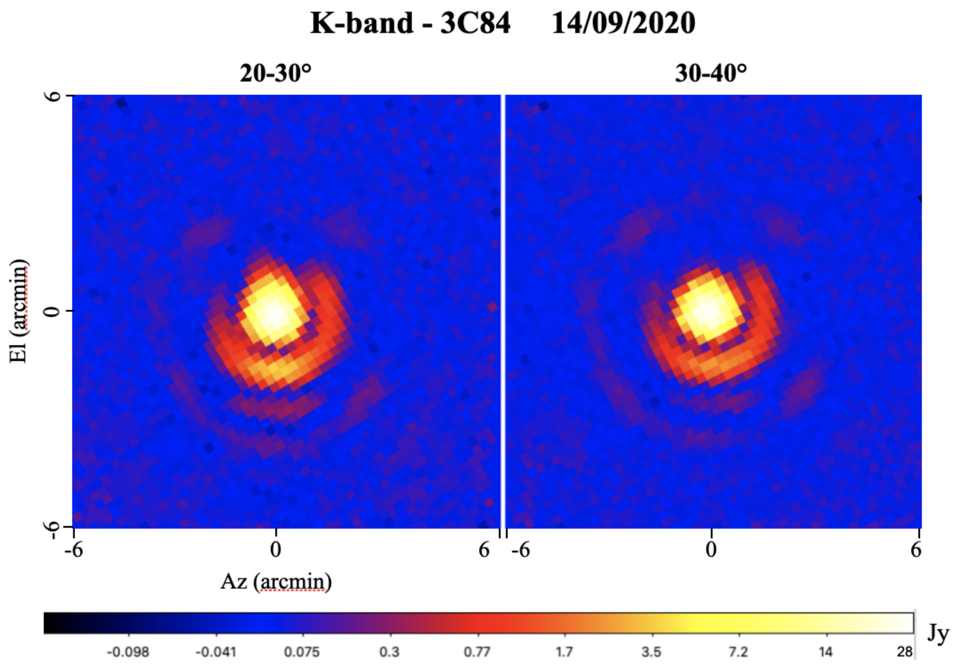

Figure 15: *Az/El maps of 3C84 in Jy at 20-30° and 30-40° of elevation obtained on 14 September 2020 at 18.7 GHz, with a pixel resolution of 0.25'.*

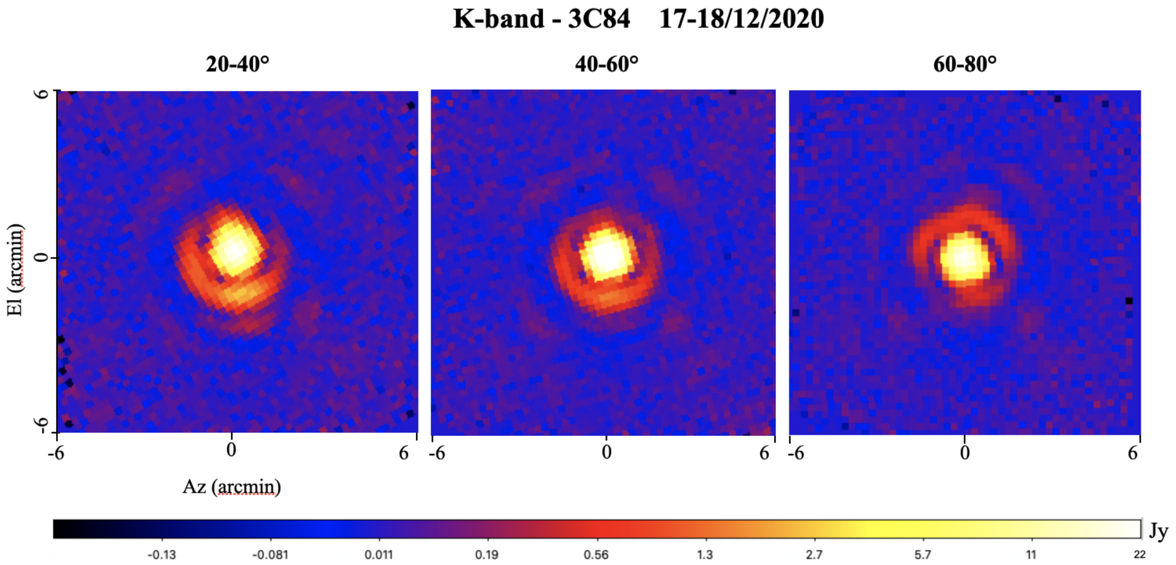

Figure 16: *Az/El maps of 3C84 in Jy at 20-40°, 40-60° and 60-80° of elevation obtained on 17-18 December 2020 at 18.7 GHz using the new M1-LUT, with a pixel resolution of 0.25'.*

We report in Tables 6a and 6b the contribution of the secondary lobes w.r.t. the central beam flux associated with 3C84. Below 30°el, we note an excess of about 13-14% (about -9 dB) in the second lobe and 15-17% in the second plus third lobes w.r.t. the flux in the central beam. The excess in the second lobe becomes < 8% (-11/13 dB) at 30-40°el, and below 3% (-15 dB) above 40°el. This asymmetry does not satisfy the SRT design specifications (secondary lobe below -20 dB; Prandoni et al. 2017).

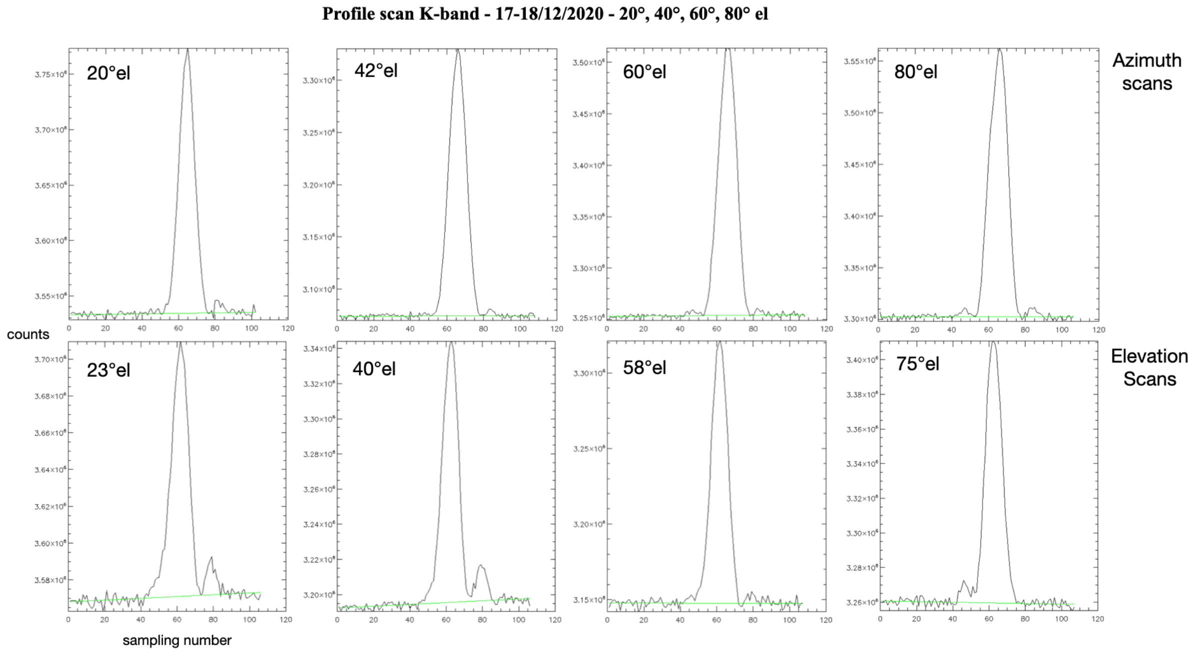

Figure 17: *Profiles of the central scans of 3C84 in azimuth (top) and elevation (bottom) for 20°, 40°, 60° and 80° elevation (from left to right) using the data obtained on 17 -18 December 2020.*

3C84 **18.7 GHz**	**Central beam** (Jy) (Gauss 2D fit)	**Central beam+ Second lobe** (Jy) **(flux excess w.r.t. central beam in % and in dB)**	**Central beam + Second +Third lobes** (Jy) **(flux excess w.r.t. central beam in % and in dB)**
20-30°	28.3	32.3 **14.1%** **-8.5 dB**	33.2 **17.3%** **-7.6 dB**
30-40°	28.3	29.7 **4.9%** **-13.1 dB**	30.4 **7.4%** **-11.3 dB**

Table 6a : *Flux density of 3C84 measured at 18.7 GHz on 14/09/2020 (flag spectral channels: 100-180, res=0.25', opacity tau=0.05) associated with the central beam (Gauss 2D fit) and with the secondary lobes (see Fig. 15).*

3C84 **18.7 GHz**	**Central beam** (Jy) (Gauss 2D fit)	**Central beam+ Second lobe** (Jy) **(flux excess w.r.t. central beam in % and in dB)**	**Central beam + Second +Third lobes** (Jy) **(flux excess w.r.t. central beam in % and in dB)**
20-30°	24.9	28.1 **12.9%** **-8.9 dB**	28.6 **14.9%** **-8.3 dB**
30-40°	23.9	25.7 **7.5%** **-11.2 dB**	26.0 **8.9%** **-10.6 dB**
40-50°	22.4	22.9 **2.2%** **-16.5 dB**	23.1 **3.1%** **-15.1 dB**
50-60°	23.9	24.2 **1.3%** **-19.0 dB**	24.4 **2.1%** **-16.8 dB**
60-70°	22.4	22.8 **1.8%** **-17.4 dB**	23.0 **2.7%** **-15.7 dB**
70-80°	22.3	23.0 **3.1%** **-15.0 dB**	23.2 **4.0%** **-13.9 dB**

Table 6b : *Flux density of 3C84 measured at 18.7 GHz on 17/12/2020 (new M1 LUT, flag spectral channels: 120-150, res=0.25', opacity tau=0.04) associated with the central beam and the secondary lobes for the different elevation ranges (Fig. 16). Note that the flux from the central beam is different from that measured on 14/09/2020. It is due to intrinsic flux variations of the source (Britzen et al. 2019).*

We measured the beam size by fitting the calibrator with a 2D Gaussian fit on the 2018 and 2020 data (Fig. 18). We considered all the dataset, including the very low elevations (below 20°) in 2018. The mean value of the beam size is 0.85' at 22 GHz, which is close to the theoretical beam size 0.84' rescaled from Bolli et al. (2015) at this frequency. Note that the only point different from the other ones corresponds to the beam size obtained at 9-12°. The beam size is instead 0.97' +/- 0.01 at 18.7 GHz (2020 data), which is also close to the theoretical beam size 0.99' at this frequency.

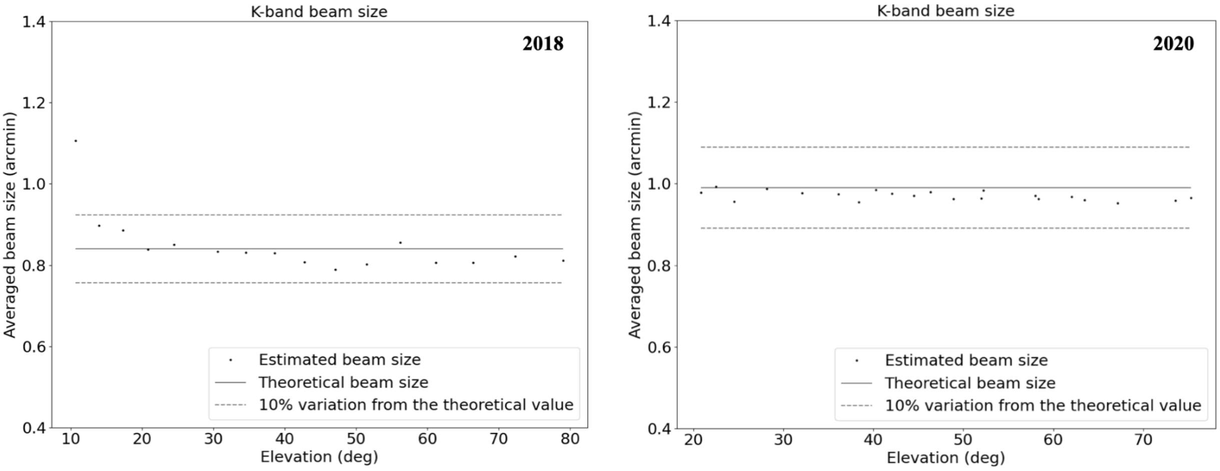

Figure 18: *K-band beam size as a function of the elevation of 3C84 at 22 GHz in 2018 (left) and at 18.7 GHz in 2020 (right). The solid lines indicate the theoretical beam size values rescaled from Bolli et al. (2015) at both frequencies, while the dashed line indicates the 10% deviation from the theoretical values.*

We measured the beam deformation in azimuth and elevation at the various elevations (see Fig. 19). In 2018, the beam deformation measured at 22 GHz is higher below 30° of elevation (about 0.12' in the 15-30° elevation range). Above 30°, we estimated a deformation of about 0.06', which corresponds to 7% of the beam. In 2020, the beam deformation is about 0.06’ (6% of the beam) at 18.7 GHz. For comparison, the beam deformation measured by Bolli et al. (2015) is shown in Fig. 20.

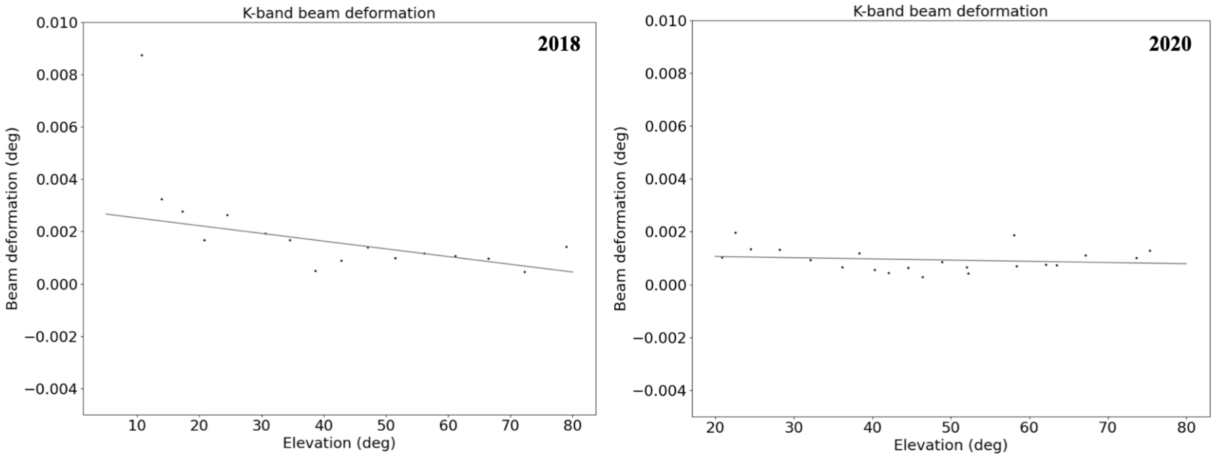

Figure 19: *K-band beam deformation measured at 22 GHz in 2018 during the recommissioning (left) and in 2020 at 18.7 GHz (right).*